Ab-initio investigation of the band alignment between Cu_2ZnSnS_4 and different buffer materials (Al_2ZnO_4, CeO_2, $ZnSnO_3$)

A. Albar[†] and U. Schwingenschlögl[*]

[†]*Jeddah University, Physics Department, Jeddah 21589, Saudi Arabia*

[*]*King Abdullah University of Science and Technology (KAUST), Physical Science and Engineering Division (PSE), Thuwal 23955-6900, Saudi Arabia*

Abstract

Limited efficiency of Cu_2ZnSnS_4 (CZTS) solar cells due to high recombination rates at the CZTS-buffer interface calls for alternative buffer materials to enhance the open circuit voltage and, therefore, the device performance. By means of ab-initio hybrid functional calculations, we investigate the interfaces between the *p*-type absorber CZTS and the *n*-type buffer materials Al_2ZnO_4, CeO_2, or $ZnSnO_3$ to evaluate the band alignment. Strong hole confinement is predicted for the CZTS/Al_2ZnO_4 and CZTS/$ZnSnO_3$ interfaces. A small conduction band offset of 0.31 eV is obtained for the CZTS/$ZnSnO_3$ interface, indicating that $ZnSnO_3$ should be considered for improving the efficiency of CZTS solar cells.

Keywords: solar cell, buffer material, conduction band offset, band alignment

[*] udo.schwingenschlogl@kaust.edu.sa

I. INTRODUCTION

While solar cells based on the absorber $Cu(In,Ga)Se_2$ achieve efficiencies that exceed those of multi-crystalline Si solar cells [1], the high price of In is a critical limitation. Therefore, recent research efforts focus on finding cheap, abundant, and environmentally friendly alternatives. Cu_2ZnSnS_4 (CZTS) is a p-type semiconductor and receives attention due to its high absorption coefficient of 104 cm^{-1} [2] and direct band gap of 1.5 eV [3, 4]. A power conversion efficiency of 8.4% has been demonstrated in Ref. [5] and hydrazine pure-solution processing of CZTS has been used in Ref. [6] to obtain a value of 12.6%. Recently, a record power conversion efficiency of more than 18% has been reported in Ref. [7], while the theoretical maximum is 32.4% [8]. For comparison, commercial solar cells reach in the lab a power conversion efficiency of 24% and typical values during field operation are 11-17% [9, 10]. At the moment, the efficiency of CZTS solar cells is mainly limited by the low open circuit voltage, a consequence of defects either in CZTS or at the interface to the buffer material (which lead to carrier loss) [11]. In the case of the CZTS/CdS interface, the critical role of the cliff-like conduction band offset (CBO) for a high recombination rate and low open circuit voltage has been discussed in Ref. [12]. While the experimental situation is still controversial, a cliff-like CBO also has been predicted by ab-initio calculations [13]. Better performance can be achieved by interfaces with spike-like CBO [14]. Experimentally, n-type CdS provides a PCE of only 12.4% even for high quality CZTS [15], demonstrating the need to explore alternative buffer materials (which ideally should not contain toxic elements).

Candidates for buffer materials must combine transparency (wide band gap; to maximize the amount of solar radiation reaching the CZTS absorber layer) with a high carrier concentration, small spike-like (positive) CBO, and large cliff-like (negative) valence band offset (VBO). A large CBO reduces the flow of photo-generated electrons (high resistance of the p-n junction) and thus lowers the efficiency of a solar cell [16–18]. Previous attempts to use ZnS, ZnSe, Zn(O,S), and In_2S_3 as buffer materials have resulted in low power conversion efficiencies (0.8% [19], 2.2% [19], 4.6% [20], and 6.9% [21], respectively) due to large CBOs (1.1 eV for ZnS [22], 0.9 eV for Zn(O,S) [23], and 0.4 eV for In_2S_3 [23]). On the other hand, first experimental results indicate that ZnO:Al [24], CeO_2 [25], and $Zn_{1-x}Sn_xO_y$ [26] have potential as buffer materials. For this reason, we use in the present study ab-initio calculations to investigate the band alignment at the interfaces between p-type CZTS and

n-type Al_2ZnO_4, CeO_2 (rutile phase), or $ZnSnO_3$, aiming at insights that can support the rational optimization of CZTS solar cells.

II. COMPUTATIONAL METHOD

The projector augmented wave method with ultrasoft pseudopotentials is used as implemented in the Vienna Ab-initio Simulation Package [27]. We employ an electronic convergence criterion of 10^{-4} eV and an atomic force convergence criterion of 0.01 eV/Å. The generalized gradient approximation of Perdew-Burke-Ernzerhof is used for structural optimization and effective mass calculations, while other properties are evaluated based on hybrid functional calculations [28]. The Hartree-Fock exchange required to reproduce the experimental band gap is 0.35 for CZTS (1.53 eV [29]), 0 for Al_2ZnO_4 (3.32 eV in the $Fd\bar{3}m$ phase [30]), 0.15 for CeO_2 (3.30 eV in the $Fm\bar{3}m$ phase [31]), and 0.35 for $ZnSnO_2$ (2.6-3.4 eV [32]). A plane wave cutoff energy of 500 eV and a Gaussian smearing of 0.05 eV width are employed. The Brillouin zone is integrated on a $5 \times 5 \times 3$ Γ-centered grid for CZTS, Al_2ZnO_4, and $ZnSnO_3$, while for CeO_2 a $5 \times 5 \times 7$ Γ-centered grid is used. CZTS is tetragonal (space group $I\bar{4}$; $a = 5.464$ Å and $c = 10.904$ Å), while Al_2ZnO_4 (space group $Imma$; $a = 5.710$ Å, $b = 5.834$ Å, and $c = 8.227$ Å) and $ZnSnO_3$ (space group $Pnma$; $a = 5.381$ Å, $b = 5.408$ Å, and $c = 7.940$ Å) are orthorhombic. For CeO_2 we address the rutile phase (space group $P4_2/mnm$; $a = 5.135$ Å and $c = 3.636$ Å), because it is stable under tension (lattice constant mismatch at the interface to CZTS) [33]. We note that the band alignment

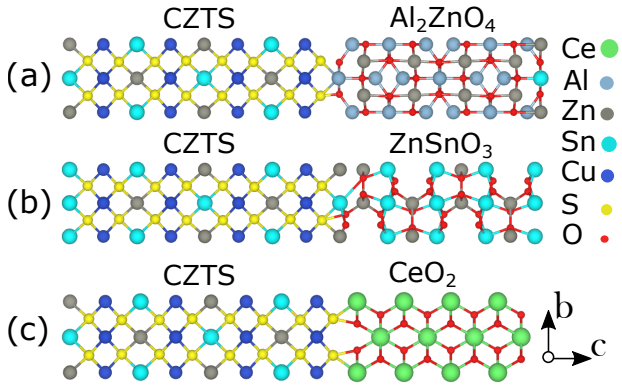

FIG. 1. Schematic structure of the (a) CZTS/Al_2ZnO_4, (b) CZTS/$ZnSnO_3$, and (c) CZTS/CeO_2 supercell.

between CZTS and CeO_2 in the fluorite phase (stable at zero pressure) has been investigated in Ref. [34].

Interfaces are built along the c-axis by placing $1\times1\times2$ (CZTS, Al_2ZnO_4, and $ZnSnO_3$) or $1\times1\times4$ (CeO_2) supercells of the bulk materials in contact with each other. Fig. 1 shows the structures of the combined supercells used for the calculations. As each material slab has a thickness of at least 15 Å, artificial interaction between an interface and its periodic images is avoided. The VBO and CBO are calculated using the potential line-up method [35–38]. We require for each material a bulk calculation to obtain the valence band maximum (VBM), size of the band gap (E_g), and macroscopic average electrostatic potential (V). Interface calculations are required to line-up the macroscopic average electrostatic potential across the interface (potential difference ΔV). We then have

$$\mathrm{VBO} = (\mathrm{VBM}^{\mathrm{buffer}} - \mathrm{V}^{\mathrm{buffer}}) - (\mathrm{VBM}^{\mathrm{CZTS}} - \mathrm{V}^{\mathrm{CZTS}}) + \Delta\mathrm{V} \tag{1}$$

and

$$\mathrm{CBO} = (\mathrm{E_g^{buffer}} - \mathrm{E_g^{CZTS}}) + \mathrm{VBO}. \tag{2}$$

III. RESULTS AND DISCUSSION

Our hybrid functional calculations result in band gaps of 1.53 eV, 3.53 eV, 3.30 eV, and 3.05 eV for bulk CZTS, Al_2ZnO_4, $ZnSnO_3$, and CeO_2, respectively, see Fig. 2 for partial

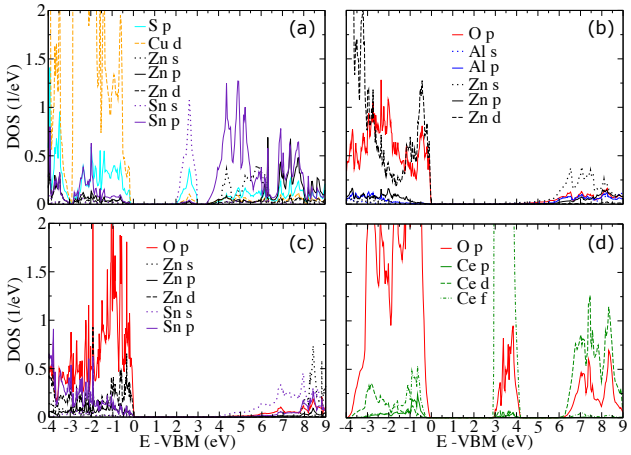

FIG. 2. Partial DOS for bulk (a) CZTS, (b) Al_2ZnO_4, (c)$ZnSnO_3$, and (d) CeO_2.

density of states (DOS) curves. For CZTS [Fig. 2(a)] the valence band edge is characterized by a low hole effective mass, as it is due to hybridized S p and Cu d states ($m_h^* = 0.6m_0$). The conduction band edge is dominated by delocalized Sn s states, which give rise to a low electron effective mass ($m_e^* = 0.2m_0$). For Al_2ZnO_4 [Fig. 2(b)] the valence band edge is due to hybridized O p and Zn d states with higher hole effective mass ($m_h^* = 3.8m_0$), as the

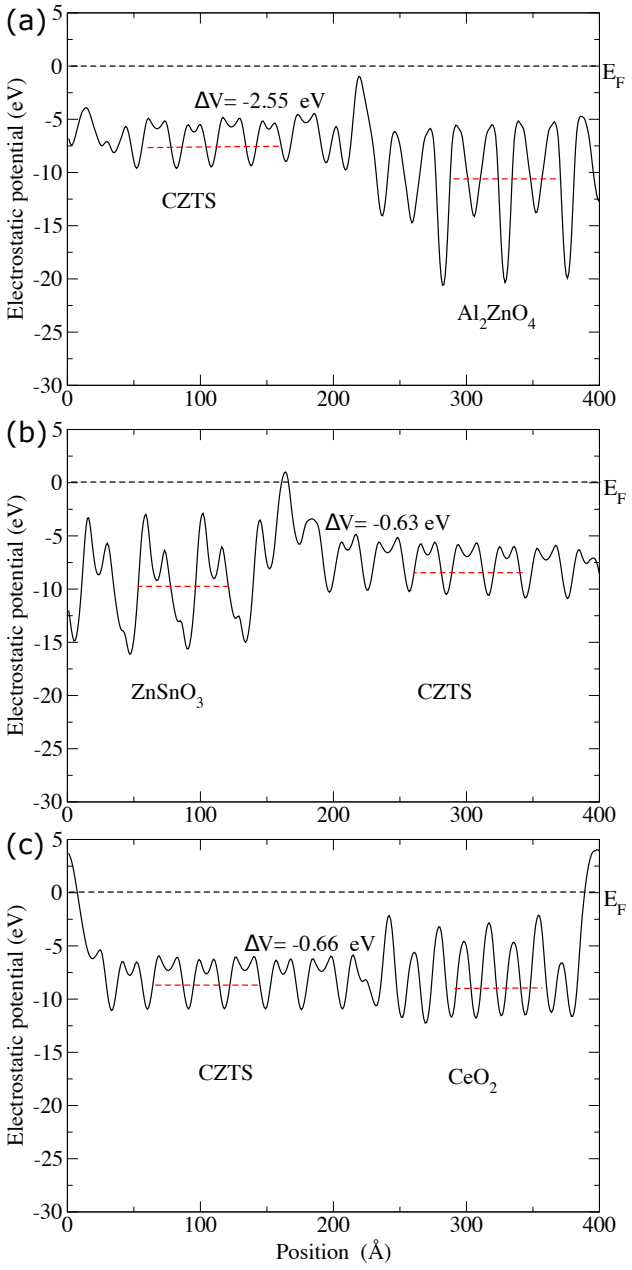

FIG. 3. Planar average (black line) and macroscopic average (red line) of the electrostatic potential for the (a) CZTS/Al_2ZnO_4, (b) CZTS/$ZnSnO_3$, and (c) CZTS/CeO_2 interface.

O $2p$ orbitals are more localized than the S $3p$ orbitals, while the conduction band edge is dominated by delocalized Zn s states ($m_e^* = 0.12m_0$). For $ZnSnO_3$ [Fig. 2(c)] the valence band edge is also due to hybridized O p and Zn d states ($m_h^* = 6.8m_0$), while the conduction band edge is dominated by delocalized Sn s states ($m_e^* = 0.3m_0$). For rutile CeO_2 [Fig. 2(d)] the valence band edge is dominated by O p states ($m_h^* = 2.4m_0$) and the conduction band edge by strongly localized Ce f states ($m_e^* = 17.9m_0$), which is similar to the fluorite phase (limited electron transport) [34].

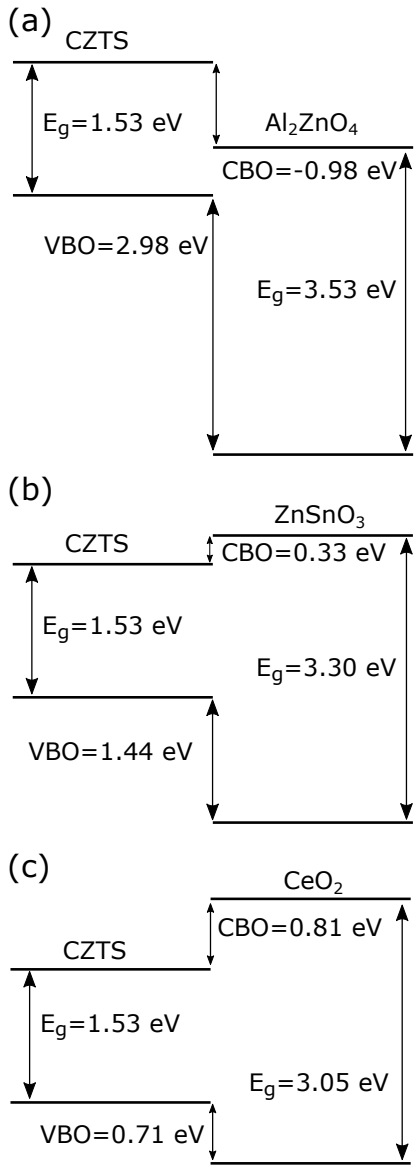

FIG. 4. Band alignment diagram for the (a) CZTS/Al_2ZnO_4, (b) CZTS/$ZnSnO_3$, and (c) CZTS/CeO_2 interface, with the obtained values of VBO, CBO, and E_g.

We now investigate the band alignment at the interfaces between CZTS and the buffer materials. For the difference between VBM and V we obtain values of 10.52 eV, 16.05 eV, 9.71 eV, and 11.89 eV for CZTS, Al_2ZnO_4, $ZnSnO_3$, and CeO_2, respectively. Averaging the electrostatic potential in planes parallel to the interface, we obtain for ΔV the values given in Fig. 3. We observe that the amount of Hartree-Fock exchange taken into account in the hybrid functional calculations has hardly any effect on these values. The VBOs and CBOs derived from Eqs. (1) and (2) are given in Fig. 4. In each case we obtain a negative cliff-like VBO. A positive spike-like CBO is found for $ZnSnO_3$ and CeO_2, and a negative cliff-like CBO for Al_2ZnO_4. At the CZTS/Al_2ZnO_4 interface the negative CBO enhances the flow of electrons (low interface resistance; enhanced recombination and reduced open-circuit voltage), while at the CZTS/CeO_2 interface the large CBO represents a potential barrier that counteracts the flow of electrons (high interface resistance). On the other hand, the small CBO (0.33 eV) at the CZTS/$ZnSnO_3$ interface suggests that $ZnSnO_3$ is a promising buffer material. The large |VBO| at the CZTS/Al_2ZnO_4 and CZTS/$ZnSnO_3$ interfaces results in confinement of holes in CZTS and thus in reduction of the recombination rate, in contrast to the small |VBO| at the CZTS/CeO_2 interface. Previous experimental work on the band alignment between CZTS and CeO_2 in the fluorite phase has reported a high power conversion efficiency of 6.6% despite a CBO of -0.12 ± 0.20 eV [34]. The fluorite-to-rutile phase transition of CeO_2 under tension [33], according to our results, would lower the efficiency significantly due to the different band alignments.

IV. CONCLUSION

In conclusion, ab-initio calculations are used to investigate the band alignment at the interfaces between the p-type absorber CZTS and the n-type buffer materials Al_2ZnO_4, CeO_2, or $ZnSnO_3$. Cliff-like (negative) VBOs are obtained for all interfaces, while strong hole confinement (reduced recombination of holes and electrons at the interface) is predicted only for the CZTS/Al_2ZnO_4 and CZTS/$ZnSnO_3$ interfaces. A cliff-like (negative) CBO at the CZTS/Al_2ZnO_4 interface enhances the recombination and reduces the open-circuit voltage, while a large spike-like (positive) CBO at the CZTS/CeO_2 interface hinders electron flow through the p-n junction and thereby limits the power conversion efficiency. The CZTS/$ZnSnO_3$ interface shows a small spike-like CBO of 0.33 eV, which indicates that

$ZnSnO_3$ is an excellent alternative buffer material for CZTS solar cells.

ACKNOWLEDGMENTS

The research reported in this publication was supported by funding from King Abdullah University of Science and Technology (KAUST). For computer time, this research used the resources of the Supercomputing Laboratory at KAUST.

---

[1] P. Jackson, R. Wuerz, D. Hariskos, E. Lotter, W. Witte and M. Powalla, Phys. Status Solidi RRL 10, 583-586, 2016.

[2] W. Xinkun, L. Wei, C. Shuying, L. Yunfeng and J. Hongjie, J. Semicond. 33, 022002, 2012.

[3] S. Schorr, M. Tovar, H. J. Hoebler and H. W. Schock, Thin Solid Films 517, 2508-2510, 2009.

[4] S. Siebentritt and S. Schorr, Prog. Photovolt. Res. Appl. 20, 512-519, 2012.

[5] B. Shin, O. Gunawan, Y. Zhu, N. A. Bojarczuk, S. J. Chey and S. Guha, Prog. Photovolt. Res. Appl. 21, 72-76, 2013.

[6] W. Wang, M. T. Winkler, O. Gunawan, T. Gokmen, T. K. Todorov, Y. Zhu and D. B. Mitzi, Adv. Energy Mater. 4, 1301465, 2014.

[7] A. D. Adewoyin, M. A. Olopade and M. Chendo, Optik 133, 122-131, 2017.

[8] W. Shockley and H.J. Queisser, J. Appl. Phys. 32, 510-512, 1961.

[9] H. Hankins, Stand-alone solar electric systems. London: Earthscan; 2010.

[10] J. Wong, R. Sridharan and V. Shanmugam, IEEE Trans. Electron Devices 62, 3750-3755, 2015.

[11] A. Polman, M. Knight, E. C. Garnett, B. Ehrler and W. C. Sinke, Science 352, 307-317, 2016.

[12] A. Santoni, F. Biccari, C. Malerba, M. Valentini, R. Chierchia and A. Mittiga, J. Phys. D 46, 175101, 2013.

[13] S. Chen, A. Walsh, J. H. Yang, X. G. Gong, L. Sun, P. X. Yang, J. H. Chu and S. H. Wei, Phys. Rev. B 83, 125201, 2011.

[14] A. Crovetto, M. L. N. Palsgaard, T. Gunst, T. Markussen, K. Stokbro, M. Brandbyge and O. Hansen, Appl. Phys. Lett. 110, 083903, 2017.

[15] M. Courel, J. A. Andrade-Arvizu and O. Vigil-Galán, Appl. Phys. Lett. 105, 233501, 2014.

[16] T. Minemoto, T. Matsui, H. Takakura, Y. Hamakawa, T. Negami, Y. Hashimoto, T. Uenoyama and M. Kitagawa, Sol. Energy Mater. Sol. Cells 67, 83-88, 2001.

[17] D. Tang, Q. Wang, F. Liu, L. Zhao, Z. Han, K. Sun, Y. Lai, J. Li and Y. Liu, Surf. Coat. Technol. 232, 53-59, 2013.

[18] T. Minemoto and M. Murata, Sol. Energy Mater. Sol. Cells 133, 8-14 2015.

[19] M. A. Akram, S. Javed, M. Islam, M. Mujahid and A. Safdar, Sol. Energy Mater. Sol. Cells 146, 121-128, 2016.

[20] T. Ericson, J. J. Scragg, A. Hultqvist, J. T. Wätjen, P. Szaniawski, T. Törndahl and C. Platzer-Björkman, IEEE J. Photovolt. 4, 465-469, 2014.

[21] F. Jiang, C. Ozaki, Gunawan, T. Harada, Z. Tang, T. Minemoto, Y. Nose and S. Ikeda, Chem. Mater. 28, 3283-3291, 2016.

[22] D. Aaron, R. Barkhouse, R. Haight, N. Sakai, H. Hiroi, H. Sugimoto and D. B. Mitzi, Appl. Phys. Lett. 100, 193904, 2012.

[23] C. Yan, F. Liu, N. Song, B. K. Ng, J. A. Stride, A. Tadich and X. Hao, Appl. Phys. Lett. 104, 173901, 2014.

[24] T. Aizawa, K. Tanaka, K. Tagami and H. Uchiki, Phys. Status Solidi C 10, 1050-1054, 2013.

[25] A. Crovetto, C. Yan, B. Iandolo, F. Zhou, J. Stride, J. Schou, X. Hao and O. Hansen, Appl. Phys. Lett. 109, 233904, 2016.

[26] M. Asaduzzaman, A. N. Bahar, M. M. Masum and M. M. Hasan, Alexandria Eng. J. 56, 225-229, 2017.

[27] G. Kresse and D. Joubert, Phys. Rev. B 59, 1758-1775, 1999.

[28] A. V. Krukau , O. A. Vydrov, A. F. Izmaylov and G. E. Scuseria, J. Chem. Phys. 125, 224106, 2006.

[29] I. G. Orletskyi, M. M. Solovan, V. V. Brus, F. Pinna, G. Cicero, P. D. Maryanchuk, E. V. Maistruk, M. I. Ilashchuk, T. I. Boichuk, and E. Tresso, J. Phys. Chem. Solids 100, 154-160, 2017.

[30] H. M. Ali, M. M. Abd El-Raheem, N. M. Megahed, and H. A. Mohamed, J. Phys. Chem. Solids 67, 1823-1829, 2006.

[31] V. V. Afanas'ev, S. Shamuilia, A. Stesmans, A. Dimoulas, Y. Panayiotatos, A. Sotiropoulos, M. Houssa, and D. P. Brunco, Appl. Phys. Lett. 88, 132111, 2006.

[32] F.-Y. Wu, J.-W. Li, Y. Qi, W.-T. Ding, Y.-Y. Guo, and Y.-W. Zhou, Acta Metall. Sin. (Engl. Lett.) 29, 827-833, 2016.

[33] T. X. T. Sayle, B. J. Inkson, A. Karakoti, A. Kumar, M. Molinari, G. Möbus, S. C. Parker, S. Seal and D. C. Sayle, Nanoscale 3, 1823-1837, 2011.

[34] A. Crovetto, C. Yan, B. Iandolo, F. Zhou, J. Stride, J. Schou, X. Hao and O. Hansen, Appl. Phys. Lett. 109, 233904, 2016.

[35] E. A. Kraut, R. W. Grant, J. W. Waldrop and S. P. Kowalczyk, Phys. Rev. Lett. 44, 1620-1623, 1980.

[36] C. G. Van de Walle and R. M. Martin, Phys. Rev. B 35, 8154-8165, 1987.

[37] R. Puthenkovilakam, E. A. Carter and J. P. Chang, Phys. Rev. B 69, 155329, 2004.

[38] P. G. Moses, M. Miao, Q. Yan and C. G. Van de Walle, J. Chem. Phys. 134, 084703, 2011.